Electro-Thermal Simulation & Characterization of a Microheater for SMO Gas Sensors

Ayoub Lahlalia, Olivier Le Neel, Ravi Shankar, Shian Yeu Kam, and Lado Filipovic

***Abstract*— The microheater is an important part of a semiconducting metal oxide gas sensor, as its primary function is to heat up the sensitive layer to a desired temperature. The operating temperature of the sensor depends on the sensitive material used and the species of the target gases. Therefore, an accurate extraction of the sensor active area temperature as a function of the applied power is critical for device characterization. These measurements are experimentally challenging due to the extremely small sensing surface area, down to a few tens of μm^2, resulting in the need to develop new measurement approaches. In this paper, quantitative testing methods based on platinum and chrome silicon (CrSi) resistance thermometry, as well as a qualitative testing method (light glow) have been carried out to measure the power consumption of two different devices. CrSi has been used as a temperature sensor due to its ability to detect temperatures above 450 °C by acting as a phase-change material. For accurate measurements of temperature distribution, the presented gas sensors are equipped with three configurations of resistive temperature detectors at different locations. To further analyze a sample closed-membrane sensor, finite-element simulations were performed and an analytical model was designed and compared with experimentals. [2017-0228]**

***Index Terms*— Microheater, electro-thermal characterization, gas sensors, semiconducting metal oxide, SnO_2, chrome silicon (CrSi).**

I. Introduction

IN THE last years, the use of gas sensors has increased sharply. This interest is mainly due to the growing importance of environmental monitoring, health care, safety, and process control. In fact, research is currently ongoing to develop a variety of gas sensors based on semiconducting sensing layers. The need to design a gas sensor with improved performance such as ultra-low power consumption, fast thermal response, high sensitivity, low cost and compatibility, is an ongoing and multi-faceted research effort.

The microheater is one of the most important and most complex components of the semiconducting metal oxide (SMO) gas sensor, defining its performance in terms of power consumption and temperature distribution. The primary function of the heater is to provide a specific temperature uniformly across an active sensing area, required for the reaction between the sensing layer and the targeted gas [1].

Metal oxide-based gas sensors, such as SnO_2, ZnO, and WO_2 have a solid track record in bulk sizes (several cm^3 and mm^3 device volumes applied in automotive and industrial applications) thanks to the material's long term stability and fast response [2], [3]. With the progress of MEMS technologies, these solid state sensors now appear to have vast potential thanks to their manufacturing capabilities in consumer products with a high level of production rates. This type of sensor is able to detect target gases at levels down to a few tens ppb in air with ultra-low power consumption [4], thereby enabling multiple applications for health and environmental protection, such as air quality monitoring based on wireless sensor networks, embedded systems, and RFID tags [5].

To improve the gas sensor performance, including the baseline stability, response time, and sensitivity, the gas sensor must operate at a controlled and uniform temperature over the entire active area, while keeping power consumption to a minimum. In order to reach this aim, materials with low thermal conductivity are recommended for use as an insulation layer, minimizing thermal dissipation from the heater to the substrate; this way the microheater is able to reach the highest possible temperature.

Most previous studies have only used a single resistive temperature detector on the membrane, neglecting that the microheater could have poor uniformity in the temperature distribution [4], [6]. Even a small change in temperature over the sensitive layer leads to baseline drift. Furthermore, working at a nonuniform temperature activates more interactions between gases and the sensitive layer, which impacts the sensitivity and selectivity of the sensor [7]. For this purpose, three resistance readouts using Pt and chrome silicon (CrSi) resistive temperature detector (RTD) configurations have been integrated onto the microheater in order to extract the temperature over the active area as a function of applied power. It should however be noted that each physical sensor is equipped with a single RTD configuration. For each configuration, the temperature was measured at a different location on the sensor. Collecting these measurements together allows us to accurately determine the temperature distribution on the microheater. In order to deal with a very small active surface area, which is a delicate task, additional approaches have been used, including analytical modeling, light glow analysis, and finite-element simulations.

To confirm the obtained results, a comparison between the analytical model, the finite-element simulations, and the

Manuscript received September 15, 2017; revised March 21, 2018; accepted April 2, 2018. Date of publication April 11, 2018; date of current version May 31, 2018. Subject Editor J. Yoon. *(Corresponding author: Ayoub Lahlalia.)*

A. Lahlalia and L. Filipovic are with the Institute for Microelectronics, Technische Universität Wien, 1040 Wien, Austria (e-mail: lahlalia@iue.tuwien.ac.at).

O. Le Neel, R. Shankar, and S. Y. Kam are with the Research and Development Department, STMicroelectronics Pte Ltd, Singapore 569508 (e-mail: olivier.leneel@st.com).

Color versions of one or more of the figures in this paper are available online at http://ieeexplore.ieee.org.

Digital Object Identifier 10.1109/JMEMS.2018.2822942

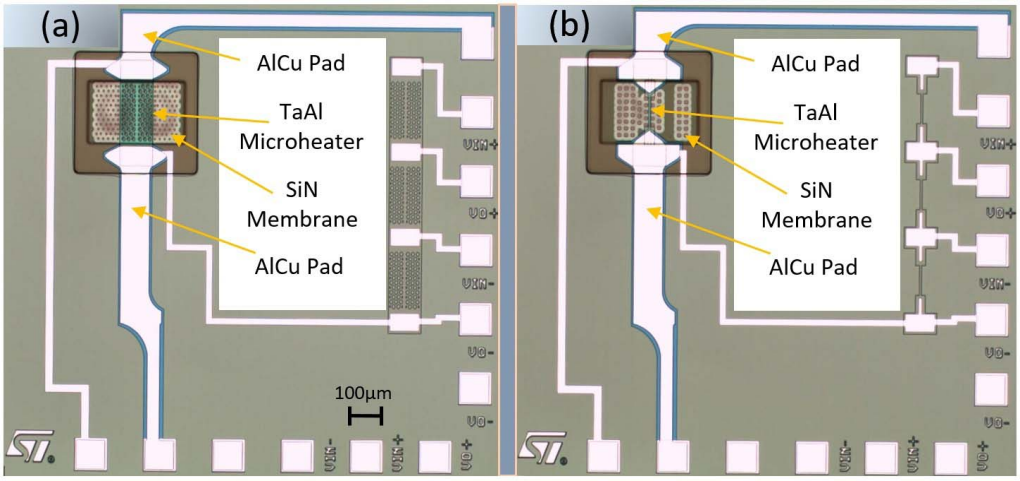

Fig. 1. Top view of the entire structure of the SMO gas sensors (a) D01 and (b) D02.

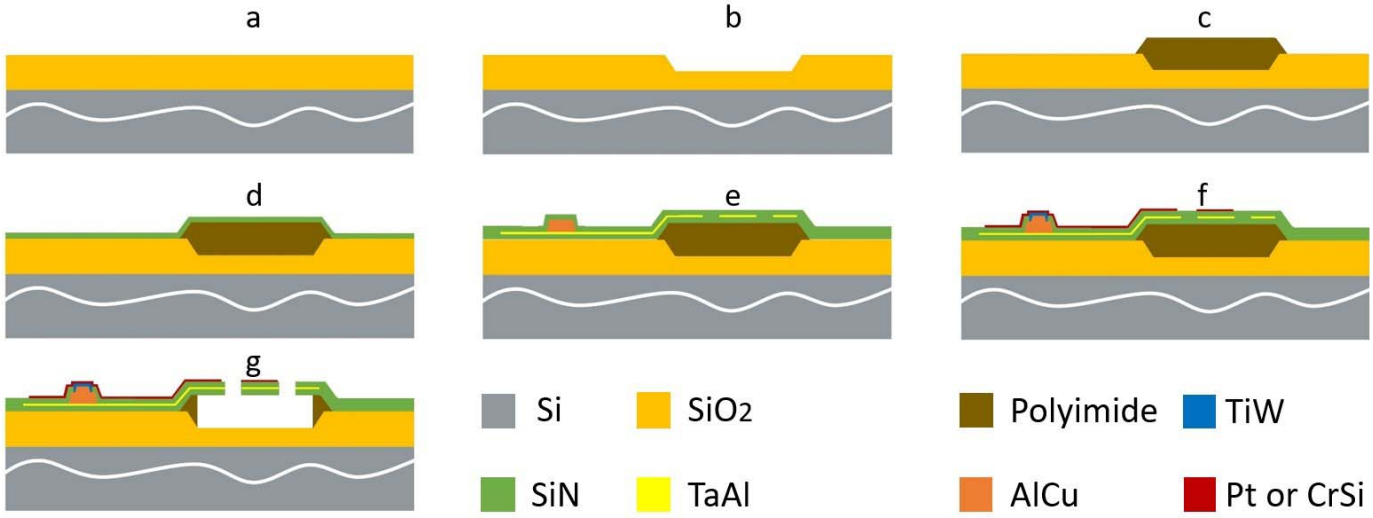

Fig. 2. The fabrication process of the microheater and RTD based SMO gas sensor. See text in Section II A for a detailed description of the fabrication process.

Pt RTD and CrSi RTD measurements have been performed. Using the numerical results, it is possible to optimize future sensor designs for improved thermal uniformity and power consumption; note that the geometrical design of the micro-heater, choice of materials, and membrane structure define the electro-thermal performance [4]. For this study, two different sensors have been used, namely D01 and D02, where each microheater is deposited onto a perforated membrane in silicon nitride as shown in Fig. 1. Microheater of D01 is a combination of small resistances created by piercing the TaAl plate, which has a size of 186μm $\times$ 100μm, while the microheater for D02 is a single beam with dimensions 100μm $\times$ 6μm. The temperature uniformity over the sensitive layer and the operation at low power consumption are vital for emerging applications of gas sensors and their integration in electronics such as smartphones and smartwatches. The aim of this work is to accurately identify the active area temperature as a function of applied power using several experimental and simulation techniques.

II. Device Fabrication

A. Sensor Fabrication Process

The structures D01 and D02 were both fabricated using a planar thin film STMicroelectronics proprietary technology [8] realized on 6" silicon wafers. The sensors fabrication process is illustrated in Fig. 2 with each device having an area of 1.9mm $\times$ 1.9mm. All of the patterning processes were performed by photolithography. A 500nm thin layer of AlCu is deposited on the sensors in order to create an electrical contact to the microheater. A 300nm thin silicon nitride layer is sandwiched between the platinum temperature sensor and Tantalum-Aluminum microheater for electrical insulation. Finally, to form the gas sensor membrane, a sacrificial polyimide was etched using selective plasma etching with the aim of achieving low power consumption and good thermal isolation.

The details of the fabrication process are as follows: A 3μm thick layer of silicon dioxide is grown by a thermal oxidation

TABLE I
PARAMETERS FOR A THERMAL EQUIVALENT ELECTRICAL CIRCUIT MODEL

Thermal parameter	Electrical equivalent	Thermal parameter	Electrical equivalent
Temperature T (K)	Voltage V (V)	Heat flow P (W)	Current I (A)
Specific heat C_p (J/Kg K)	Permittivity ε (F/m)	Thermal conductivity k (W/K m)	Electric conductivity σ (S/m)
Thermal resistivity ρ_{th} (K m/W)	Electric resistivity ρ_{el} (Ω m)	Heat Q (J = W s)	Charge Q (C = A s)
Resistance R_{th} (K/W)	Resistance R (Ω = V/A)	Capacitance C_{th} (J/K)	Capacitance C (F)

process at 1100°C (Fig. 2a), followed by wet chemical etching of the oxide using hydrogen fluoride (HF) (Fig. 2b). The etching is isotropic and is timed to etch 2μm deep. For the formation of the sacrificial polyimide, HD8820 is spin coated to a thickness of 6μm. The photo-patternable polyimide is exposed with UV light using a mask and the exposed regions is developed away (Fig. 2c). To get the desired thickness of 3μm, the polyimide is cured in oven for 1h at 350°C. A plasma enhanced chemical vapor deposition (PECVD) is carried out to deposit a 500nm layer of silicon nitride (Fig. 2d). A 160nm TaAl layer was subsequently deposited on the electrical insulator by MRC star. The Tantalum-Aluminum microheater was patterned using photolithography and etched by AME8330/2200W in a BCl_3, Cl_2 and CHF_3 plasma chemistry. A 500nm AlCu is sputtered in a MRC tool using a physical vapor deposition (PVD) process, and the pattering of the conductive pads is done by using photoresist followed by wet etching. An additional 300nm thin silicon nitride layer is deposited to encapsulate the Tantalum-Aluminum microheater (Fig. 2e). For thermal characterization the gas sensor fabrication is limited to 3 stacked layers: the microheater, the insulating layer, and the temperature sensor. To measure the temperature more accurately, two different temperature sensitive films are deposited using PVD at low temperature and power in order to obtain the desired thickness, conductivity, and uniformity. For this purpose, in several devices a titanium tungsten/platinum (TiW/Pt) layer is deposited on top of the Si_3N_4 by MRC Star at room temperature. The TiW layer is used as an adhesion layer between the insulation and platinum. Other devices have a 40nm thin layer of chrome silicon instead of platinum and was deposited by Endura 5500 with an RF power of 100W. The sheet resistances of Pt and CrSi are measured to be 5Ω/sq and 11kΩ/sq at room temperature, respectively. A photoresist is spun on the wafer and patterned using photolithography. The platinum and chrome silicon layers are subsequently etched using Tegal6540/600W/150W in Cl_2 and Ar plasma chemistries (Fig. 2f). After opening the holes in the Si_3N_4 membrane by dry etching using a CH_4, CHF_3, and Ar plasma, the polyimide is etched using an additional plasma etching step to create a closed membrane, on which the sensor structure is placed, as shown in Fig. 2g [9]. The wafers are finally annealed in a 20% oxygen environment at 400°C for 1h in order to stabilize the final structure.

B. Material Properties

The use of Tantalum-Aluminum (TaAl) as a microheater material is appropriate, since it is able to retain its mechanical strength at high temperatures. Furthermore, the microheater resistance does not change as a function of temperature [10], unlike with platinum, which is a commonly used material for microheater fabrication. According to our experimental measurements, the TaAl temperature coefficient of resistance (TCR) is about -100ppm/°C, allowing for the microheater to provide a stable temperature as a function of input power and to minimize the effects of hot spots [11].

For gas sensor fabrication, an additional thin film of platinum or chrome silicon is added for thermal characterization. Pt is chosen as a temperature sensor due to its linear resistance variation versus temperature [12], while the CrSi resistance as a function of temperature can vary drastically and its conductivity can change permanently due to changes in its material structure [13]. This CrSi property, which is linked to material stoichiometry, is employed here as a calibration method. Among its other features, it is compatible with semiconductor thin film PVD processes and has a tailorable TCR based on material composition. Nevertheless, the temperature extraction with CrSi is not highly accurate since the material composition can change from wafer to wafer, which influences the calibration results.

III. ELECTRO-THERMAL MODEL

A. Heat Transfer Model

The thermal behaviour of the SMO gas sensor can be described using various equivalent circuit models. In this paper, a Cauer model, applied to study the thermal performance of design D02 is presented, allowing to estimate the power consumption and the thermal response of the sensor as a function of applied power.

Heat conduction and convection processes can be modeled using three important material parameters: the thermal resistance R_{th}, the thermal capacitance C_{th}, and the convection resistance R_{conv}. Furthermore, in order to facilitate model implementation, we note that each thermal parameter has an analogous electrical equivalent as shown in Table 1. To switch from a thermal model to an electrical model, each layer or each component of the sensor is represented by a thermal resistances R_{th} in parallel with the thermal capacitance C_{th}. This is the case for all layers except for the microheater element, which is applied as a current source, since conductive current is analogous to thermal power (Table 1), and the heated surfaces in contact with air, which are described by convection resistances. The equations used to determine the thermal resistance, thermal capacitance, and convection resistance are

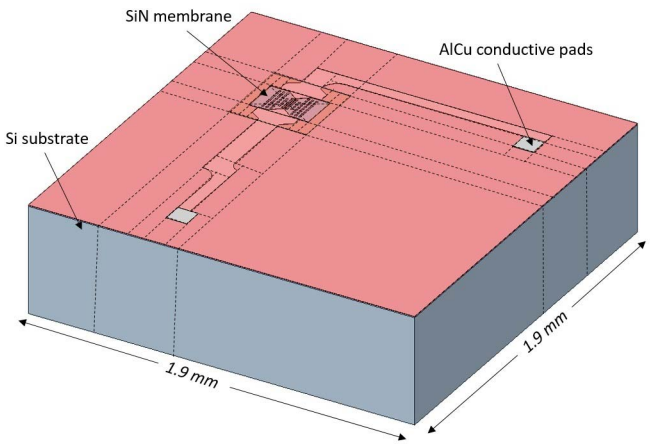

Fig. 3. Approach used to describe and model the entire gas sensor D02. Each layer of the gas sensor is discretized into small rectangular blocks as represented here by the dotted lines.

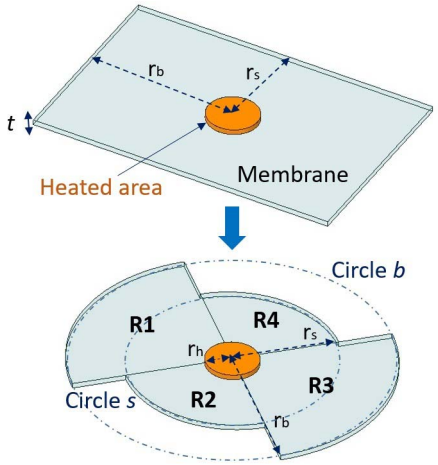

Fig. 4. Sensor geometry, when considering heat loss by conduction through the membrane.

given by (1), (2), and (3), respectively:

$$R_{th} = \frac{t}{k \cdot A} \tag{1}$$

$$C_{th} = c \cdot \rho \cdot V \tag{2}$$

$$R_{conv} = \frac{1}{h \cdot A_r}. \tag{3}$$

For the thermal resistance (1), t is the thickness of the layer, k is the thermal conductivity, and A is the cross-sectional area normal to the heat flow. For the thermal capacitance (2), c is the specific heat, ρ is the material density, V is the volume of the material. For the convection resistance (3), h is the heat transfer coefficient and A_r is the exposed area from which the heat flows, given in m^2.

The same principle for calculating electrical parameters can be applied to the entire sensor as shown in Fig. 3. The length, and width of the membrane are 290μm and 186μm, respectively, while the microheater has an area of 100μm $\times$ 6μm. In order to avoid increasing the model complexity, we focus solely on the Cauer network model of the membrane, which is responsible for a major share of the power consumption. To further support the analytical model, the power consumption of the entire sensor, obtained by finite-element simulations and experimental measurements are compared with analytical results.

B. Heat Conduction Through the Membrane

For the calculation of heat conduction through the closed membrane, a novel simplified model is used by replacing the rectangular membrane with two circular bow-tie membranes, as shown in Fig. 4. This allows for a one-dimensional treatment of the problem, using cylindrical coordinates. The membrane has been divided into 4 thermal resistances R1, R2, R3, and R4 from Fig. 4. Each resistance represents the heat losses through one quarter of the cylinder with radius of r_b or r_s less one quarter of the heated volume of the heated area. Regarding the heat losses through the suspended membrane, another model is presented in our previous work [14].

Considering the heat conduction problem in cylindrical coordinates [15], thermal resistances can be calculated as follows:

$$R_1 = R_3 = \frac{\ln(r_b/r_h) \cdot 2}{\pi \cdot k \cdot t} \tag{4}$$

$$R_2 = R_4 = \frac{\ln(r_s/r_h) \cdot 2}{\pi \cdot k \cdot t} \tag{5}$$

where r_h is the radius of the heated area, r_b and r_s are the radii of circles b and s from Fig. 4, respectively.

It can be observed from (4) and (5) that heat losses through the membrane can be reduced by choosing a ratio r_b/r_h and r_s/r_h as large as possible, meaning choosing a small microheater in comparison to the membrane size. Furthermore, thin membrane layers and low thermal conductivity are highly recommended to further decease the power consumption. However, its should be noted that the mechanical performance of the membrane at high temperatures must also be considered during sensor design, which leads to a trade-off between low power consumption and high mechanical reliability of the sensor.

C. Heat Losses to the Air

Heat losses to the surrounding air can be described by two mechanisms: convection by heat transfer due to fluid motion and conduction through the air. In order to calculate the thermal losses to the air, a simplification is required, by considering the heated membrane area as a horizontal plate of characteristic size l. This leads to the calculation of the mean heat transfer coefficient h_m, described in more detail in [14], as follows:

$$h_m = \frac{k(T_m)}{l} 0.766 (f_1(Pr) \cdot (T_{hot} - T_a) \cdot g \cdot l^3)^{1/5} \tag{6}$$

with

$$f_1(Pr) = \frac{\beta_\infty}{v^2} Pr \cdot f_2(Pr) \tag{7}$$

$$f_2(Pr) = [1 + (\frac{0.322}{Pr})^{11/20}]^{-20/11} \tag{8}$$

where Pr is the Prandtl numbers, $k(T_m)$ is the thermal conductivity of the air at $T_m = (T_{hot} + T_a)/2$, where T_a is

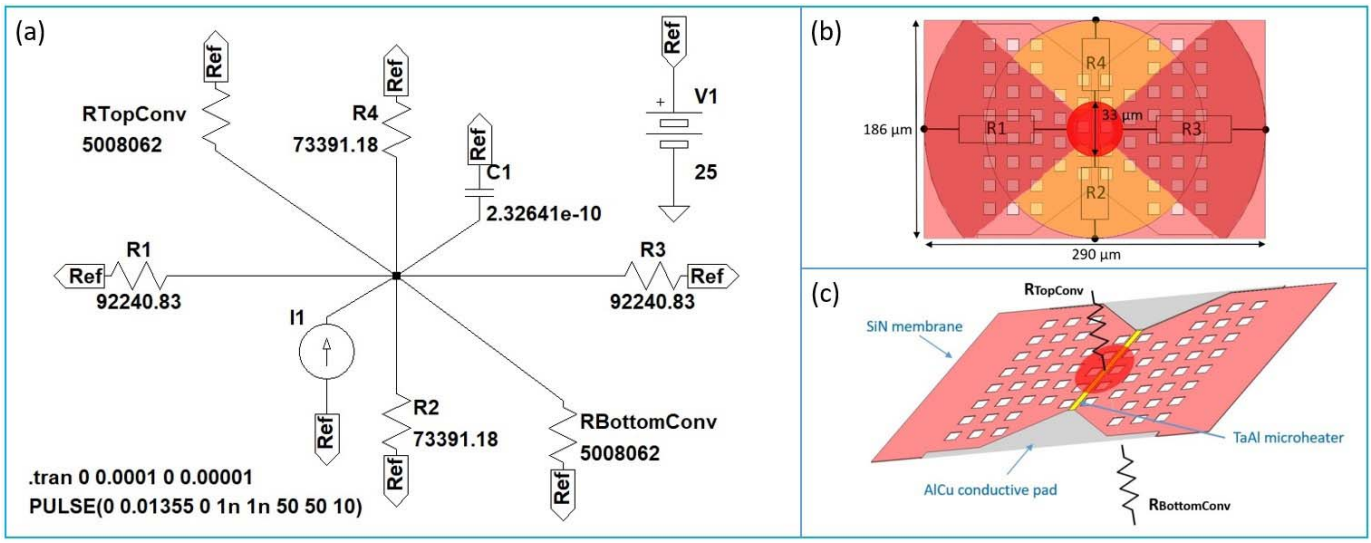

Fig. 5. (a) Electro-thermal model of the closed membrane of the sensor D02, (b) the dimensions of the membrane structure, and (c) the heat loss in membrane by convection.

the ambient temperature, g is the acceleration due to gravity, β_∞ is the thermal expansion coefficient, and υ is the kinematic viscosity. Further explanations and a detailed derivation of (6), (7), and (8) can be found in [14].

D. Electro-Thermal Model Analysis

The electro-thermal model of the membrane has been analyzed using LTspice in order to calculate the power consumption of the sensor [16]. It should be mentioned that some simplifications were made: the heated area (with a temperature uniformity within ±10°C) occupies a circle with a diameter approximately one third of the microheater length. In our example, with a 100μm microheater length, a circular uniform heated area with a diameter of 33μm was observed. This can be verified by simulations and experimental measurements based on when microheater glowing begins; only electrical losses by heating the microheater are considered; the substrate temperature is not influenced by the heated area; the membrane is treated as a simple sheet without holes; vertical heat losses are neglected due to the small thickness of the sensor layers; to calculate the mean heat transfer coefficient, the diameter of the heated area is considered as the characteristic size of the horizontal plate; heat losses by convection on the top and bottom surfaces of the membrane (heated area) are treated as identical.

Using (3),(4),(5), and (6), the numerical value of the thermal resistance and thermal capacitance, as well as the convection resistance of the electro-thermal model, can be calculated as follows:

$$R_1 = R_3 = \frac{\ln(145\mu\text{m}/16.5\mu\text{m}) \cdot 2}{\pi \cdot 30 \cdot 0.5\mu\text{m}} = 92\text{k}\Omega \tag{9}$$

$$R_2 = R_4 = \frac{\ln(93\mu\text{m}/16.5\mu\text{m}) \cdot 2}{\pi \cdot 30 \cdot 0.5\mu\text{m}} = 73\text{k}\Omega \tag{10}$$

$$h_m = \frac{0.03516}{33\mu\text{m}} 0.766(19775058.48 \cdot (275) \cdot 9.8 \cdot 33\mu\text{m}^3)^{1/5} = 233.46\text{W/m}^2\text{K}. \tag{11}$$

At this stage we can calculate the convection resistances of the top and bottom membrane surfaces (heated area) R_{TC} and R_{BC}, respectively, using (3)

$$R_{TC} = R_{BC} = \frac{1}{233.46 \cdot \pi \cdot (16.5\mu\text{m})^2} = 5\text{M}\Omega. \tag{12}$$

Now we can solve for the thermal capacity of the heated area C_{th-a} using (2)

$$C_{th-a} = 170 \cdot 3200 \cdot \pi \cdot 16.5\mu\text{m}^2 \cdot 0.5\mu\text{m} = 0.23\text{nF}. \tag{13}$$

Numerical values of the functions $f_1(Pr)$ and $k(T_m)$ are taken from [14].

The electro-thermal model equivalent of the membrane sensor D02 along with its parameters are given in Fig. 5. As shown in Fig. 5a, the electrical ground is fixed at 25V, which corresponds to a temperature of 25°C, by an extra DC source, considered as a reference reflecting room temperature. To analyze the electrical circuit, 13.55mA, which corresponds to 13.55mW power, needs to be applied in order to reach the target temperature of 300°C; this was done in LTspice by introducing an ideal current source. In the circuit, the current corresponds to the heat flow and the voltage corresponds to temperature as described in Table 1. In fact, analyzing the voltage evolution as a function of current allows to estimate the power consumption of the gas sensor. Concerning the thermal time constant of the TaAl microheater, the heated area reaches 300°C within 42μs and cools back down to room temperature in less than 38μs.

IV. Temperature Sensor Simulation & Characterization

A. FEM Simulation

To further support experimental measurements, sensor D01 and D02 have been designed and meshed with a modeling tool and simulated in a finite element environment with optimized parameters using Comsol Multiphysics [17]. The boundary conditions were initially set to 25°C for the

TABLE II
MATERIAL PROPERTIES USED IN THE SIMULATIONS

Parameters	TaAl	Si_3N_4	SnO_2	Polyimide	SiO_2	Si	AlCu
Thermal conductivity (W m^{-1} K^{-1})	240	30	64	0.14	1.4	150	240
Density (Kg m^{-3})	10^4	3200	6950	1200	2400	2300	2700
Specific heat (J Kg^{-1} K^{-1})	600	170	1000	1090	1000	710	915
Thickness (μm)	0.16	0.5 / 0.3	0.1	4	3	525	0.5

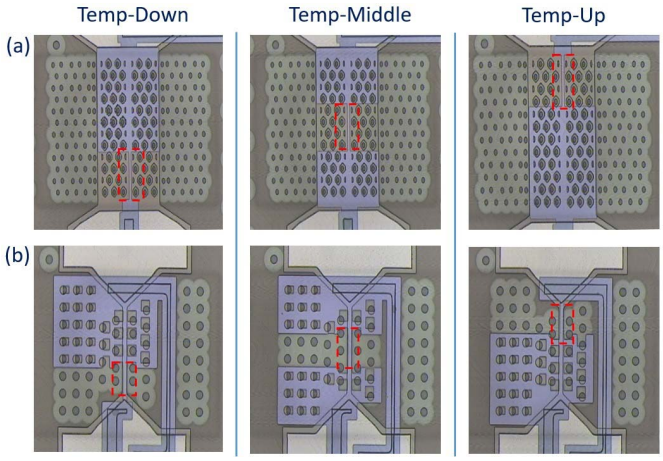

Fig. 6. Location of different RTD resistances on the microheater in (a) D01 and (b) D02 sensor designs.

surrounding temperature and gas sensor materials, while tantalum-aluminium TCR and the temperature of the substrate bottom were fixed at -100ppm/°C and 25°C, respectively. The parameters of the different layers of the entire gas sensor used in simulations, such as material properties and layer thicknesses, are given in Table 2. Regarding the heat losses to the air, 233.46 $Wm^{-2}K^{-1}$ was used for heat transfer coefficient for the front side and back side of the membrane (heated area) when the microheater temperature reaches 300°C. This value was calculated from (6) and (11) and for consistency is used in both the analytic model and finite element simulator.

Several RTD configurations have been applied and measured for sensors D01 and D02 in order to extract the precise active area temperature. Using this data, the electro-thermal simulations for the sensors can be appropriately calibrated. Since the temperature is not uniform over the microheater, three Pt RTD configurations have been used at different locations over the insulation layer as shown in Fig. 6. Temp-Up, Temp-Middle, and Temp-Down correspond to temperature measurements at the top-most, center, and bottom-most extremities of the microheater, respectively. CrSi RTD has been deposited in the same locations as Pt RTD in several samples.

B. Calibration

A simple method to extract the active area temperature based on calibrating the RTD versus the microheater temperature in a uniform temperature environment has been employed. Temperature dependences of resistance of a platinum RTD were measured in the range of 25°C up to 150°C using a Temptronic temperature controller and an Agilent 4155 parametric tester. Using these experimental measurements from different samples, the TCR of the Pt was calculated. The average value found was 1403 ppm/°C.

To measure the phase change point of CrSi, multiple wafers coated with 10% silicon and 85% chrome were heated from 50°C up to 550°C with step of 50°C in a fanned convection oven. CrSi resistance was measured by PROMETRIX OMNIMAP RS35C at 25°C after heating the wafers to the desired temperature. From our experiments, it was found that CrSi resistance at 25°C decreases significantly and irreversibly after heating the wafers above 450°C.

C. Measurements & Results

The microheater element and RTD were connected with probes using APS03 for a characterization of the electro-thermal parameters. Electrical measurements were performed at standard room conditions, where I-V curves of the TaAl microheater and RTD were measured at different power consumption by Parameter Analyzer Agilent 4155C. The initial resistance of the microheater and Pt RTD (Temp-Middle) were 290Ω and 60Ω, respectively. Using the calculated TCR and the measured resistances of CrSi RTD and Pt RTD at different power levels, the microheater temperature as a function of applied power was determined.

Fig. 7 shows the temperature distribution versus the applied microheater power. According to experimental measurements, the temperature is highest at the centre of the microheater. This result is in good agreement with finite-element simulations, as shown in Fig. 7c. In fact, low uniformity in temperature distribution over the microheater was observed for both designs. The difference in temperature between the center and extremities for D01 and D02 were 50°C and 78°C, respectively, at 300°C. On the other hand, the heater temperature reaches 300°C when 2.36V are applied, generating a 36.5mA current, and 86mW power consumption for D01; similarly, 1.78V are applied to D02, resulting in a 6.5mA current and 11.6mW power consumption.

Fig. 8 shows the measured resistance from D02 of the CrSi RTD (Rs_0) at 25°C each time the material is heated to a specific temperature, while Rs is the CrSi resistance measured as a function of applied power to the microheater. The CrSi RTD is located at the centre of the microheater (Temp-middle). According to experimental measurements, CrSi Rs_0 decreases significantly and irreversibly when the microheater consumes more than 21.2mW, which corresponds to an augmentation

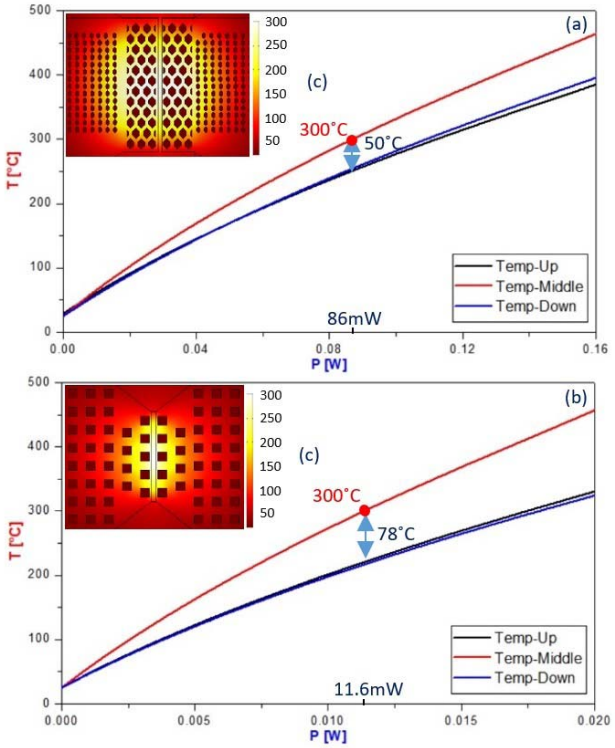

Fig. 7. Temperature distribution vs. microheater power supply for a) D01 and b) D02 sensor designs. c) Numerical simulation were performed using Comsol Multiphysics.

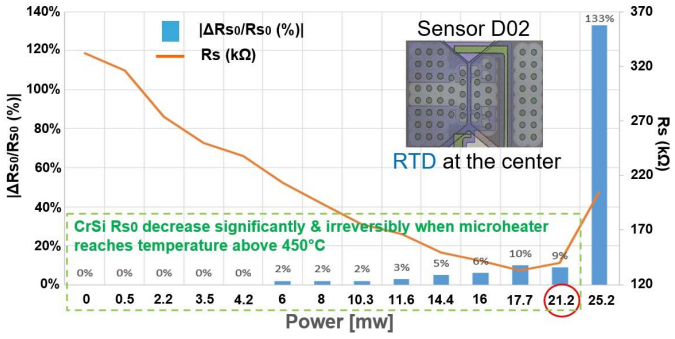

Fig. 8. Measured Rs_0 and Rs of CrSi RTD after and during heating the microheater to different temperatures, respectively.

in $|(\Delta Rs_0/Rs_0)(\%)|$ by 133%. Using measurements made directly from wafers coated with CrSi, a significant decrease in Rs_0 occurs when wafers are heated to temperatures above 450°C, which means 21.2mW power consumption corresponds to a 450°C microheater temperature.

For a quick comparison between both designs in terms of power consumption, a very simple microheater characterization in steady state has been performed: the applied voltage is slowly ramped up until we see the microheater glowing. Using this method the design with the lowest power consumption can be determined since it starts to glow at a lower temperature. For D01 the emission light of the device is observed at a bias voltage of 3.2V, corresponding to a power of 186mW, and for D02, 2.7V was required, resulting in a 26.43mW power consumption. The microheaters have a bright orange color as

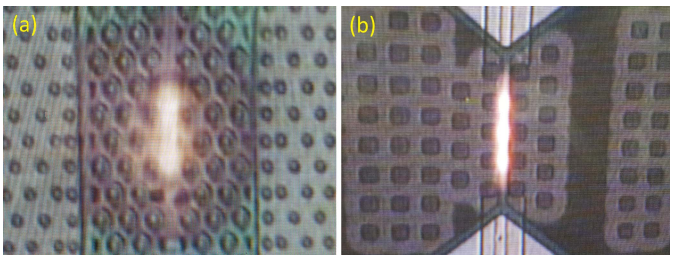

Fig. 9. (a) D01 and (b) D02 sensor designs glowing at a typical temperature 600°C.

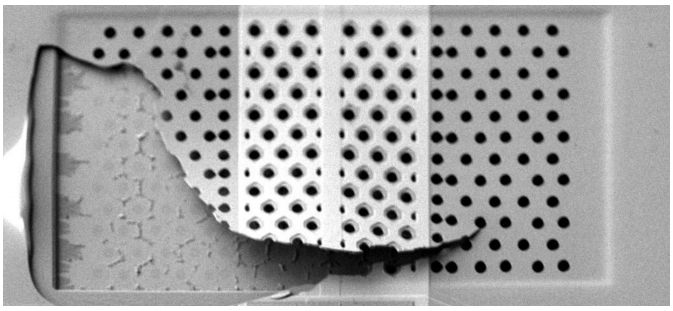

Fig. 10. Membrane of the sensor D01 after failure when operating at high temperature in the range of 700°C.

shown in Fig. 9 when the temperature is above 600°C. The heater of D01 fails at 244mW, while D02 fails at 34.9mW due to crack build-up in the membrane caused by thermal stress, which eventually leads to the heater delamination as shown in Fig. 10. This test demonstrates that the thermal stability of the designed microheater is sufficient for an optimal operation of the gas sensor between 250°C and 450°C, but that it cannot handle temperatures much higher than this.

V. Discussion

Five methods to thermally characterize the microheater for SMO gas sensors were presented. These methods are useful in extracting the active area temperature and calculating the temperature as a function of applied power to the microheater. An accurate characterization of the electro-thermal performance of the microhotplate for SMO gas sensors, including the active area temperature and thermal losses are very important for accurate reliability studies and ultimately for the optimization of sensor design with improved sensor features. To further verify the obtained results, a comparison between analytical modelling based on the Cauer network, light glow qualitative measurements, finite-element simulations, and experimental measurements using Pt RTD and CrSi RTD have been performed. The experimental measurements of RTD (Temp-Middle) show a total power consumption of 86mW for D01 and 12 mW for D02, in good agreement with the simulations and the analytical model.

Fig. 11 depicts the resulting temperature evolution as a function of applied power for D02 using the various previously described methods. According to RTD readings, the heater temperature reaches 300°C with 11.6mW power consumption with a Pt RTD and 13.5mW with a CrSi RTD. Simulations and

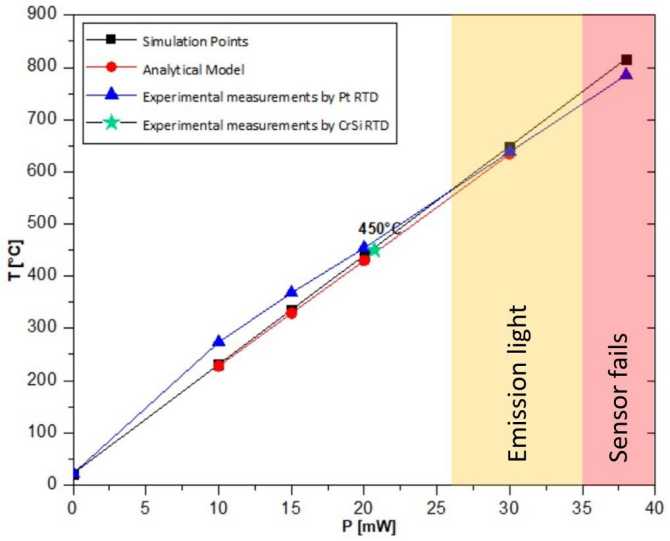

Fig. 11. Temperature as a function of applied power to the microheater of the D02 design.

analytical modelling give a power consumption of 13.3mW and 13.55mW, respectively. It should be noted that the model is useful only for specific designs which match the simplifications mentioned earlier; therefore, the power consumption of sensor D01 cannot be calculated in the same way since the electrical losses through the small resistances of the microheater are very high and the substrate is not completely insulated from the heated area. The small difference between measurements made by Pt RTD and other methods is due to the higher accuracy of Pt RTD and simplifications made in the electro-thermal model. The resulting average power consumption of the sensor D02, when considering the different methods is 13mW for 300°C.

VI. Conclusion

A systematic comparison of different methods for obtaining the microheater temperature as a function of applied power using simulations and experimental characterization have been conducted. Two different designs were used for these comparisons.

The different methods used generate similar results on the set of test circuits used. Therefore, the choice of a suitable method to be used by the technology or product designer can be recommended as follows:

- Cauer model required several steps of elementary components tuning, and there is a high risk of error due to the complexity; this method is also more complex to use and therefore more suitable for experienced sensor developers. However, the electro-thermal model gives an approximate result based only on material properties and sensor dimensions without any additional expenses through hardware or paid software resources.
- Multiphysics simulations require minimal effort after the computer aided design (CAD) of the sensor structure. Furthermore, such simulations provide a geographical temperature distribution that allows to observe the precise heat uniformity on desired locations.
- The RTD measurements provide precise and fast results, provided that the RTD layer's volume/design and position are comparable to the position of the sensing element. This technique requires as a prerequisite: the capability to deposit and etch such materials in a compatible manner to the sensor fabrication.
- The light glow technique has demonstrated a very fast, easy, and efficient qualitative method that can be used to compare the emission versus the heater power of different designs or process variations. However, this process is very limited and cannot tell us the exact power/temperature relationship the way previous methods could. It can only be used to assess the difference in power performance between various designs.

The different techniques are all demonstrated to be suitable and precise enough to be used as a tool-kit for microheater and sensor developers.

Acknowledgment

The work has been supported by the Research and Development Department at STMicroelectonics Pte Ltd Ang Mo Kio, Singapore, which has performed the sensor design, fabrication, and measurements.

References

[1] G. Cardinali *et al.*, "A smart sensor system for carbon monoxide detection," *Analog Integr. Circuits Signal Process.*, vol. 14, no. 3, pp. 275–296, 1997.
[2] M. Ortel, Y. S. Trostyanskaya, and V. Wagner, "Spray pyrolysis of ZnO–TFTs utilizing a perfume atomizer," *Solid-State Electron.*, vol. 86, pp. 22–26, Aug. 2013.
[3] G. E. Patil, D. D. Kajale, V. B. Gaikwad, and G. H. Jain, "Spray pyrolysis deposition of nanostructured tin oxide thin films," *ISRN Nanotechnol.*, vol. 2012, Jun. 2012, Art. no. 275872.
[4] I. Elmi, S. Zampolli, E. Cozzani, F. Mancarella, and G. C. Cardinali, "Development of ultra-low-power consumption MOX sensors with ppb-level VOC detection capabilities for emerging applications," *Sens. Actuat. B, Chem.*, vol. 135, no. 1, pp. 342–351, Dec. 2008.
[5] S. Zampolli *et al.*, "Ultra-low-power components for an RFID tag with physical and chemical sensors," *Microsyst. Technol.*, vol. 14, nos. 4–5, pp. 581–588, 2008.
[6] J. Spannhake *et al.*, "SnO_2: Sb—A new material for high-temperature MEMS heater applications: Performance and limitations," *Sens. Actuat. B, Chem.*, vol. 124, no. 2, pp. 421–428, 2007.
[7] N. Yamazoe and N. Miura, "Some basic aspects of semiconductor gas sensors," *Chem. Sensor Technol.*, vol. 4, pp. 19–42, Mar. 1992.
[8] R. Shankar, O. Le Neel, T.-C. Loh, and S.-Y. Kam, "Integrated SMO gas sensor module," U.S. Patent 0031506 A1, Jul. 17, 2014.
[9] T. C. Loh and O. Le Neel, "Suspended membrane device," U.S. Patent 9000542 B2, May 31, 2013.
[10] H. W. Pötzlberger, "Thin film integrated RC-networks with compensated temperature coefficients of R and C," *Active Passive Electron. Comp.*, vol. 4, nos. 3–4, pp. 139–142, 1977.
[11] P. Bhattacharyya, "Technological journey towards reliable microheater development for MEMS gas sensors: A review," *IEEE Trans. Device Mater. Rel.*, vol. 14, no. 2, pp. 589–599, Jun. 2014.
[12] S. Toskov, R. Glatz, G. Miskovic, and G. Radosavljevic, "Modeling and fabrication of Pt micro-heaters built on alumina substrate," in *Proc. 36th Int. Spring Seminar Electron. Technol. (ISSE)*, May 2013, pp. 47–52.
[13] J. L. Gonzalez-Vidal, A. Reyes-Barranca, M. de la L. Olvera, A. Maldonado, and W. Calleja-Arriaga, "Smart sensors, actuators, and MEMS II," *Proc. SPIE*, vol. 5836, p. 746, Jul. 2005.
[14] A. Lahlalia, L. Filipovic, and S. Selberherr, "Modeling and simulation of novel semiconducting metal oxide gas sensors for wearable devices," *IEEE Sensors J.*, vol. 18, no. 5, pp. 1960–1970, Mar. 2018.
[15] H. Baehr, K. Stephan, *Wärme-und Stoffübertragung*, 3rd ed. Berlin, Germany: Springer, 1998.

[16] Linear Technology Corporation, California, USA. *LTspice*. Accessed: Jun. 2017. [Online]. Available: www.linear.com/solutions/ltspice
[17] *COMSOL Multiphysics*, COMSOL AB, Stockholm, Sweden, 2016.

Ayoub Lahlalia received the M.Sc. degree in microsensors and detection systems from Aix-Marseille University, Marseille, France, in 2016. He is currently pursuing the Ph.D. degree with the Institute for Microelectronics, TU Wien. He joined the Institute for Microelectronics in 2017, as a Research Project Assistant. His scientific interest focuses on gas sensors simulation, characterization, and data processing.

Olivier Le Neel received the Ph.D. degree in physics from the University of Rennes, Rennes, France, in 1991. Since 2007, he has been a Senior Technology Manager with STMicroelectronics Pte Ltd, Ang Mo Kio, Singapore.

Ravi Shankar received the M.Tech. degree in solid-state materials from the Indian Institute of Technology, Delhi, India, in 1999. He is currently a Project Leader with the Technology and Business Development Department, STMicroelectronics Pte Ltd, Ang Mo Kio, Singapore.

Shian Yeu Kam received the B.E. degree from the National University of Singapore in 2005. Since 2005, he has been a Staff Process Engineer with STMicroelectronics Pte Ltd, Ang Mo Kio, Singapore.

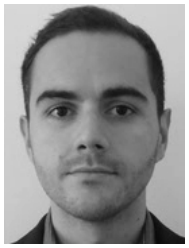

Lado Filipovic received the B.E. degree in electrical engineering and the master's degree in applied sciences from Carleton University, Ottawa, ON, Canada, in 2006 and 2009, respectively, and the Ph.D. degree in technical sciences from the Institute for Microelectronics, TU Wien, in 2012, under the supervision of Prof. S. Selberherr. In 2010, he joined the Institute for Microelectronics, TU Wien. The main focus of his research is design and simulation of environmental sensors and, more specifically, metal oxide semiconductor gas sensors for the detection of toxic gases and pollutants.